Physical and Chemical Properties of MoP, Ni_2P, and MoNiP Hydrodesulfurization Catalysts: Time-Resolved X-ray Diffraction, Density Functional, and Hydrodesulfurization Activity Studies

José A. Rodriguez,* Jae-Yong Kim, and Jonathan C. Hanson
Department of Chemistry, Brookhaven National Laboratory, Upton, New York 11953

Stephanie J. Sawhill and Mark E. Bussell*
Department of Chemistry, MS-9150, Western Washington University, Bellingham, Washington 98225

Received: December 21, 2002; In Final Form: April 15, 2003

Synchrotron-based time-resolved X-ray diffraction was used to study in situ the crystalline phases present during the preparation of bulk and silica-supported MoP, Ni_2P, and MoNiP by reduction of oxidic precursors in hydrogen. Independent of the type of oxidic precursor used or the presence of silica as a support, the formation of the metal phosphides occurs at temperatures between 600 and 800 °C. Since the common species in all the cases are phosphate-type groups (PO_x), it seems that their reduction by hydrogen is the final and determining step in the formation of MoP, Ni_2P, and MoNiP. Silica-stabilized phosphide phases were detected during the synthesis of Ni_2P/SiO_2 and MoP/SiO_2 catalysts. In the case of Ni_2P/SiO_2, before the appearance of the final phosphide, strong diffraction lines are observed for $Ni_{12}P_5$. First-principles density functional calculations for bulk MoP, Ni_2P, and MoNiP indicate that the Ni−P and Mo−P bonds in these compounds have a small degree of ionic character. For MoP, Ni_2P, and MoS_2 a correlation is found between the electronic properties of the metal cations and their hydrodesulfurization activities when supported on silica. Surprisingly, a $MoNiP/SiO_2$ catalyst is much less active than either MoP/SiO_2 or Ni_2P/SiO_2 catalysts.

I. Introduction

Since the last century petroleum has been a very important source of fossil fuels and chemical feedstocks.[1] The fuels derived from petroleum contribute approximately one-third to one-half of the world's energy supply and are used not only for transportation but also to heat buildings.[1] Sulfur-containing compounds are common impurities in all crude oil. In our industrial society, these impurities have a negative impact in the processing of oil-derived chemical feedstocks and degrade the quality of the air by forming sulfur oxides (SO_x) during the burning of fuels and by poisoning the catalysts in vehicle catalytic converters.[1,2] In petroleum refineries, organosulfur compounds are converted to H_2S and hydrocarbons by reaction with hydrogen over a catalyst (hydrodesulfurization process).[1,3,4] The sulfides of many hydrogenating metals are active for hydrodesulfurization (HDS), and catalysts containing cobalt, molybdenum, nickel, and tungsten are widely used on a commercial basis.[1,3−5] More stringent environmental regulations stress the need to develop a new generation of HDS catalysts that lead to the ultimate goal of clean-burning fuels.[6]

Several articles have recently appeared in the literature describing the HDS properties of metal phosphide catalysts.[7−10] Silica-supported molybdenum (MoP/SiO_2)[7d,9] and nickel phosphide (Ni_2P/SiO_2)[8a,8c,8d,10] catalysts have shown particular promise, with activities similar to or higher than those of sulfide-based catalysts. For example, in a recent study a 30 wt % Ni_2P/SiO_2 catalyst prepared by hydrogen reduction of an oxidic precursor was 15 and 3.5 times more active than sulfided Mo/SiO_2 and $Ni-Mo/SiO_2$ catalysts, respectively, after 100 h on stream.[10] Characterization with X-ray diffraction (XRD) and transmission electron microscopy (TEM) confirmed the presence of Ni_2P crystallites dispersed on the surface of the silica support.[10] Given the need to develop highly active HDS catalysts to meet requirements for lower sulfur levels in fuels combined with the prospect of processing lower quality petroleum feedstocks,[8,10] further investigation of phosphide-based hydrotreating catalysts is needed to understand and evaluate their properties. An important issue in the preparation of these systems is the type of phosphide phase formed as a function of temperature and how this is affected by the oxide support. Phosphide↔oxide interactions can enhance the stability of phosphide phases which are metastable or unimportant for the unsupported material.

In this article, we also compare the HDS activity of silica-supported MoP, Ni_2P, and MoNiP catalysts. Surprisingly, a $MoNiP/SiO_2$ catalyst is much less active than either MoP/SiO_2 or Ni_2P/SiO_2 catalysts. In first-principles density functional calculations a correlation is found between the electronic (density of states near the Fermi level, metal centers charge) and chemical (HDS activity) properties of these phosphides. Time-resolved XRD is used to study in detail the crystalline phases present during the preparation of bulk and supported phosphide catalysts from oxidic precursors. The structural properties of these systems are examined as a function of temperature. Investigations at Brookhaven National Laboratory have established the feasibility of conducting subminute, time-resolved XRD experiments under a wide variety of temperature and pressure conditions (−190 °C < T < 900 °C; P < 45 atm).[11] This important advance results from combining the high intensity of synchrotron radiation with rapid new parallel data-collection devices. Time-resolved XRD has recently being used to study the kinetics of the reduction of several oxides (NiO,[12]

* Corresponding authors.

10.1021/jp022639q CCC: $25.00
Published on Web 06/11/2003

$NiMoO_4$,[13] CeO_2,[14] CuO[15]) with hydrogen, and thus, it is ideal for examining the synthesis of metal phosphides via the reaction of oxidic precursors with H_2 plus the role of phosphide↔oxide interactions.

II. Experimental Methods

II.1. Catalyst Preparation. The syntheses of bulk and silica-supported Ni_2P and MoP has recently been described elsewhere, and the preparation of the oxidic precursors of these catalysts are only briefly outlined here.[9,10] A more detailed description is presented for the synthesis of bulk and silica-supported MoNiP.

Oxidic Precursors of Ni_2P and Ni_2P/SiO_2. For the oxidic precursor of Ni_2P, an aqueous solution containing $Ni(NO_3)_2 \cdot 6H_2O$ (Alfa Aesar, 99.9985%) and $(NH_4)_2HPO_4$ (Mallinckrodt, 99.9%) was stirred overnight and then heated to 87 °C for approximately 48 h, yielding a greenish yellow precipitate which was collected by filtration and dried at 100 °C; Gopalakrishnan et al.[16] identified the solid product prepared by a similar procedure to be $NH_4NiPO_4 \cdot nH_2O$. The oxidic precursor of a 25 wt % Ni_2P/SiO_2 catalyst was prepared by impregnation of the silica support (SiO_2, Cab-O-Sil, M-7D grade, 200 m^2/g) with aqueous solutions of $Ni(NO_3)_2 \cdot 6H_2O$ (Alfa Aesar, 99.9985%) and $NH_4H_2PO_4$ (Baker, 99.1%). The nickel solution was added dropwise to 5.0 g of calcined silica (500 °C, 3 h) until incipient wetness, followed by drying at 120 °C, and calcination in air at 500 °C for 3 h. The support was subsequently impregnated with the $NH_4H_2PO_4$ solution and dried at 120 °C to give a precursor having a molar ratio of Ni/P = 1.25.

Oxidic Precursor of MoP and MoP/SiO_2. For the oxidic precursor of MoP, a mixture of ammonium heptamolybdate $(NH_4)_6Mo_7O_{24} \cdot 4H_2O$ (Alfa Aesar) and of diammonium hydrogen phosphate $(NH_4)_2HPO_4$ (Alfa Aesar) was dissolved in deionized water. A white solid (Mo/P = 1) obtained following evaporation of the water was calcined in air at 500 °C for 5 h to give a dark blue solid. For the oxidic precursor of a 40 wt % MoP/SiO_2 catalyst, an impregnating solution consisting of $(NH_4)_6Mo_7O_{24} \cdot 4H_2O$ and $(NH_4)_2HPO_4$ (Mo/P = 1) was added dropwise to calcined silica until incipient wetness. The precursor was dried in a 120 °C oven, and calcined in air at 500 °C for 3 h.

MoNiP and $MoNiP/SiO_2$. A procedure for the synthesis of unsupported MoNiP was recently described by Stinner et al.[17] An aqueous solution of $(NH_4)_6Mo_7O_{24} \cdot 4H_2O$ and $(NH_4)_2HPO_4$ (Mo/P = 1) was mixed with an aqueous solution of $Ni(NO_3)_2 \cdot 6H_2O$ (Ni/Mo = 1), which resulted in the formation of a green precipitate. The mixture was stirred overnight, following which the solid was collected and then dried in a 120 °C oven for 24 h. The solid was then calcined in air at 500 °C for 5 h to give the oxidic precursor of MoNiP that was used for the time-resolved XRD studies as well as the temperature-programmed-reduction (TPR) synthesis of MoNiP described below. Approximately 0.5 g of the oxidic precursor was placed in a quartz U-tube and subjected to a 300 sccm flow of H_2 (Airgas, 99.999%) while heating from room temperature to 650 °C (1 °C/min). Following TPR, the sample was cooled to room temperature in flowing H_2, flushed with 60 sccm He (Airgas, 99.999%) for 15 min, and passivated in a 60 sccm flow of 1.0 mol % O_2/He for 2 h. The He and H_2 were purified prior to use by passing through 5A molecular sieve (Alltech) and O_2 (Oxyclear) purification traps.

For the oxidic precursor of $MoNiP/SiO_2$, calcined silica was impregnated with an aqueous solution of $Ni(NO_3)_2 \cdot 6H_2O$ and $(NH_4)_6Mo_7O_{24} \cdot 4H_2O$ (Ni/Mo =1) and then dried at 120 °C for 24 h. The dried solid was subsequently impregnated with an aqueous solution of $(NH_4)_2HPO_4$ (Mo/P = 1), dried at 120 °C for 24 h, and then calcined at 500 °C for 3 h in air to give the oxidic precursor of a 25 wt % $MoNiP/SiO_2$ catalyst. The catalyst was reduced and passivated as described above for unsupported MoNiP.

II.2. Catalyst Characterization. *X-ray diffraction.* X-ray diffraction (XRD) patterns of MoNiP and $MoNiP/SiO_2$ catalysts were acquired on a Rigaku Geigerflex powder diffractometer using the Vaseline smear method. The diffractometer is outfitted with a Cu Kα source (λ = 1.5418 Å), and is interfaced to a personal computer for data acquisition and analysis using Materials Data Incorporated (MDI) DataScan and Jade Plus 5.0 software.

BET Surface Area and Chemisorption Measurements. BET surface area measurements were obtained using a Micromeritics PulseChemisorb 2700 apparatus. Approximately 0.10 g of catalyst was placed in a quartz U-tube and degassed at room temperature in a 60 sccm He flow for 30 min. This was followed by a 2 h degassing of the sample in a 45 sccm flow He at 350 °C and cooling to room temperature under flowing He. The BET measurements were carried out as described previously.[18]

Oxygen (O_2) pulsed chemisorption measurements were also carried out using the Micromeritics PulseChemisorb 2700 instrument. Chemisorption capacity measurements were conducted using a 10.3 mol % O_2/He mixture (Airco). Approximately 0.10 g of catalyst was degassed in 60 sccm He at room temperature for 30 min and then reduced by heating from room temperature to 400 °C (6.3 °C/min) in 60 sccm H_2 and holding for 2 h. The reduced samples were degassed in 60 sccm He at 400 °C for 1 h prior to chemisorption measurements. The O_2 chemisorption capacity measurements were carried out at −77 °C using a procedure published elsewhere.[18] The He and H_2 were purified prior to use by passing through 5A molecular sieve (Alltech) and O_2 (Oxyclear) purification traps.

II.3. Thiophene HDS Activity Measurements. Thiophene HDS activity measurements were carried out using an atmospheric pressure flow reactor which has been described in detail elsewhere.[18] Activity measurements were carried out at a reaction temperature of 370 °C using a reactor feed consisting of a 3.2 mol % thiophene/H_2 mixture. Prior to the activity measurements, the phosphide catalysts were subjected to a degas in 60 sccm He at room temperature for 30 min. While continuing the He flow, the temperature was adjusted to the reaction temperature of 370 °C (23 °C/min) and the flow was switched to the 3.2 mol % thiophene/H_2 reactor feed (50 sccm). The reaction was carried out for over 100 h, with automated sampling of the gas effluent occurring at 1 h intervals. Thiophene (Th) HDS activities (nmol of Th/(g of cat.·s)) were calculated from the total product peak areas calculated from the chromatogram after 100 h of reaction time.

Thiophene HDS activities were also measured for sulfided Mo/SiO_2 (30.4 wt % MoO_3) and $Ni-Mo/SiO_2$ (7.9 wt % NiO, 30.4 wt % MoO_3, Ni/Mo = 0.5) catalysts under the same reaction conditions as those employed for the activity measurements of the phosphide catalysts. The preparation of these catalysts has been described in detail elsewhere.[10]

II.4. Time-Resolved XRD Experiments. The time-resolved X-ray diffraction data were collected on beam line X7B of the National Synchrotron Light Source (NSLS).[11,19−21] In the experiments dealing with the synthesis of the bulk and supported metal phosphides, the oxidic precursors were loaded into an open sapphire capillary that was attached to a flow-reaction cell similar to those described in refs 22 and 23. The capillary was

connected to 1/16 in. Swagelok style fittings with Vespel ferrules. A 0.010 in. chromel−alumel thermocouple was inserted straight into the capillary near the oxidic precursor.[22] The sample was heated using a small resistance heater wrapped around the capillary. Diffraction patterns were recorded at temperatures in the range 25−950 °C under a 5% H_2/95% He gas mixture (flow rate = 10−20 sccm). A MAR345 detector was used to record the in situ XRD data. The typical time required for collecting an individual diffraction pattern was in the range of 0.5−2 min. The powder rings (λ = 0.9200 Å) were integrated using the FIT2D code.[24] Calculated patterns were obtained with the program GSAS[25] in a manner similar to that followed in a previous work.[26,27]

II.5. First-Principles Density Functional Calculations. In section III.4, density functional (DF) calculations with the CASTEP (Cambridge Serial Total Energy Package) suite of programs[28] are used to investigate the electronic properties of bulk Ni_2P, MoP, and MoNiP. In this code, the Kohn−Sham implementation of DF theory is used to obtain the total energy of the system. CASTEP has an excellent track record in accurate prediction of geometry and energetics for inorganic compounds.[20,27,28b,29,30] In this code, the wave functions of valence electrons are expanded in a plane wave basis set with *k*-vectors within a specified energy cutoff E_{cut}. Tightly bound core electrons are represented by nonlocal ultrasoft pseudopotentials.[34] Brillouin zone integration is approximated by a sum over special *k*-points chosen using the Monkhorst−Pack scheme.[35] In all the calculations, the kinetic energy cutoff E_{cut} (400 eV) and the density of the Monkhorst−Pack *k*-point mesh {a 4 × 4 × 5 grid for Ni_2P and MoNiP and a 7 × 7 × 6 grid for MoP} were chosen sufficiently high to ensure convergence of the computed structures and electronic properties. The exchange-correlation contribution to the total electronic energy was treated in a generalized gradient corrected (GGA) form of the local density approximation (LDA): Perdew−Burke−Ernzerhoff functional.[36] The structural parameters of the bulk phosphides in their different configurations were determined using the Broyden−Fletcher−Goldfarb−Shanno (BFGS) minimization technique, with the following thresholds for the converged structures: energy change per atom less than 5×10^{-6} eV, residual force less than 0.02 eV/Å, the displacement of atoms during the geometry optimization less than 0.001 Å, and the root mean square of the stress tensor less than 0.1 GPa. For each optimized structure, the partial charges on the atoms were estimated by projecting the occupied one-electron eigenstates onto a localized basis set with a subsequent Mulliken population analysis.[37,38] Mulliken charges have well-known limitations,[39] but are nevertheless useful as a qualitative tool to study trends in charge distribution.

III. Results

III.1. Synthesis of Ni_2P and Ni_2P/SiO_2 Catalysts: Time-Resolved XRD Studies. The top of Figure 1 displays a series of powder diffraction patterns recorded during the heating of a compound of the $NH_4NiPO_4 \cdot nH_2O$ type[10,16] from 25 to 800 °C (rate 15 °C/min) under a gas mixture of 5% H_2/95% He (flow ~ 20 sccm). In the bottom panel of the figure are shown the corresponding signals measured with a mass spectrometer for water and ammonia at the exit of the reaction cell. Initially, one sees the XRD pattern for the oxidic precursor. From 200 to 400 °C, there is evolution of water and ammonia into the gas phase. Near 400 °C, the sample becomes amorphous and all of the diffraction lines disappear. Thus, the removal of NH_3 and H_2O leads to a collapse in the structure of the oxidic precursor but no nickel phosphide is yet formed. This is most likely due to the fact that the precursor still contains significant numbers of ammonium and phosphate groups. These are removed in the temperature range 650−800 °C, and clear diffraction lines for Ni_2P[40] emerge. By 800 °C, only the diffraction pattern of Ni_2P is observed. Cooling to room temperature and subsequent reheating in flowing He did not induce the appearance of new diffraction lines.

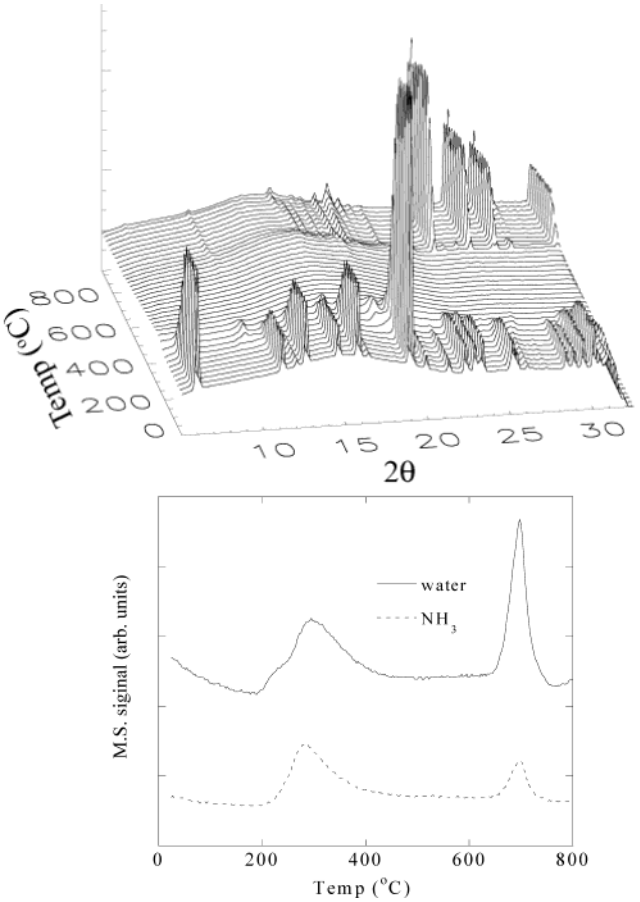

Figure 1. Top: Time-resolved powder diffraction patterns (λ = 0.9200 Å) for the reduction of $NH_4NiPO_4 \cdot nH_2O$ in a mixture of 5% H_2−95% He. Heating rate ~ 15 °C/min. The sample was taken from 25 to 800 °C and in the final step was cooled to room temperature. Bottom: MS signal as a function of temperature for the evolution of water and ammonia.

In Figure 1, the desorption of water and ammonia could be a consequence of the simple thermal decomposition of the oxidic precursor or the result of the reduction of the precursor by hydrogen. In Figure 2, we show time-resolved XRD data for the heating of $NH_4NiPO_4 \cdot nH_2O$ in a pure stream of He. Any changes seen here come from decomposition of the compound. From 25 to 450 °C, the results are very similar to those obtained in Figure 1: evolution of water and ammonia is observed and there is a breakdown in the crystal structure producing an amorphous material. From 400 to 600 °C, there is no desorption of water or ammonia, but around 600 °C diffraction lines appear that do not match those of Ni_2P[40] but instead can be assigned to α-$Ni_2P_2O_7$.[41]

In another experiment, α-$Ni_2P_2O_7$ (formed by heating the oxidic precursor in flowing He) was heated from 25 to 800 °C under a 5% H_2/95% He gas mixture (flow ~ 20 sccm); see Figure 3. Until 600 °C there was no evolution of water or ammonia and the intensity of the diffraction lines for α-$Ni_2P_2O_7$ was essentially constant. At this temperature, the desorption of water and ammonia begins while simultaneously the diffraction

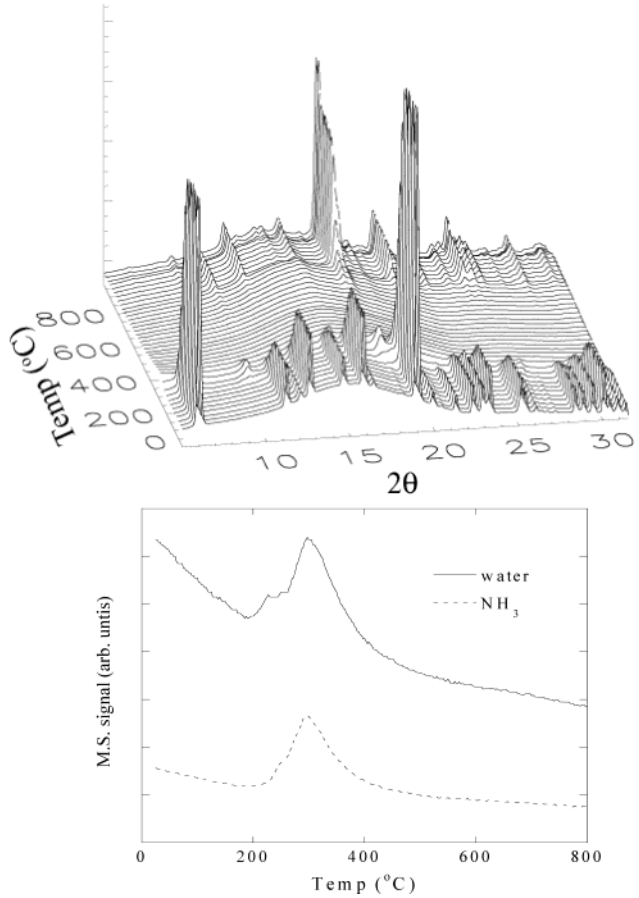

Figure 2. Top: Time-resolved powder diffraction patterns ($\lambda = 0.9200$ Å) for the heating of $NH_4NiPO_4 \cdot nH_2O$ in a flow of pure helium. Heating rate ~ 15 °C/min. Bottom: Evolution of water and ammonia as a function of temperature.

pattern for α-$Ni_2P_2O_7$ starts to disappear as Ni_2P is formed. After comparing the results in Figures 1−3, one can conclude that the first important transformation in Figure 1 (300−400 °C) is due to decomposition of $NH_4NiPO_4 \cdot nH_2O$, and that in the second (650−750 °C) the reduction of the precursor with hydrogen actually occurs to form Ni_2P.

We also examined the formation of silica-supported Ni_2P (25 wt % phosphide loading). The corresponding precursor was heated from 25 to 800 °C in an atmosphere of 5%H_2/95% He. The results of time-resolved XRD in Figure 4 indicate that NiO[42a] is present on the silica support below 400 °C and then Ni[42b] forms, followed by $Ni_{12}P_5$,[42c] and, similar to the case of unsupported Ni_2P, Ni_2P begins to form above 600 °C. A strong peak for water desorption is found at ~700 °C, probably as a consequence of the reduction of PO_x groups on the surface of the oxide support. In the mass spectrometer, the desorption of water was accompanied by a weaker signal for the desorption of ammonia.

III.2. Synthesis of MoP and MoP/SiO_2 Catalysts: Time-Resolved XRD Studies. The oxidic precursor for the synthesis of bulk MoP was heated (25−1000 °C, 15 °C/min) under a gas mixture of 5% H_2/95% He (~20 sccm). The time-resolved XRD data in Figure 5 show that around 350 °C the diffraction lines for the precursor, $Mo(OH)_3PO_4$,[43a] disappear and a nearly amorphous material is obtained, with weak diffraction lines for MoO_3.[43b] Evolution of water and ammonia is observed in broad peaks from 600 to 1000 °C. In the range 600−700 °C diffraction lines for MoO_2[43c] appear, replacing those of MoO_3,[43b] and by 800 °C the diffraction pattern of MoP[9,44] is very clear. No

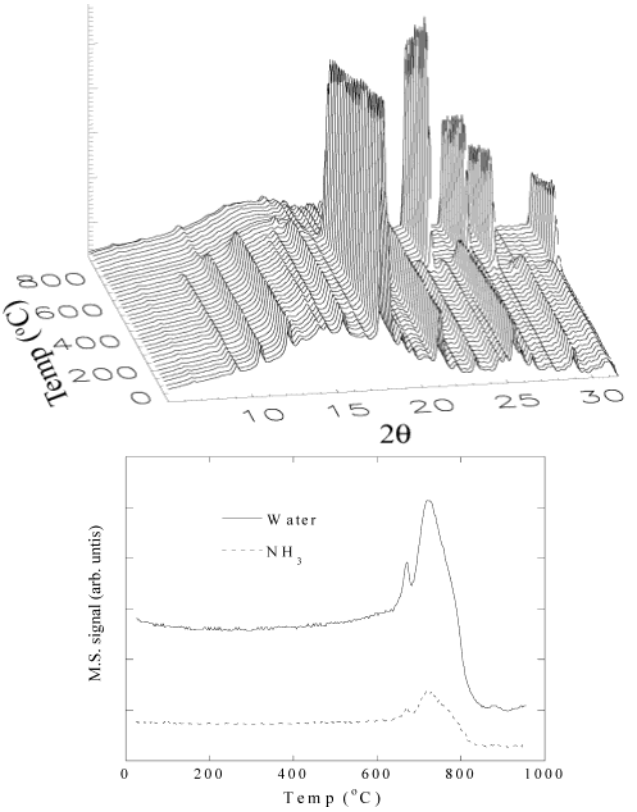

Figure 3. Top: Time-resolved powder diffraction patterns for the reduction of α-$Ni_2P_2O_7$ in a mixture of 5% H_2−95% He. Heating rate ~ 15 °C/min. Bottom: MS signal as a function of temperature for the evolution of water and ammonia.

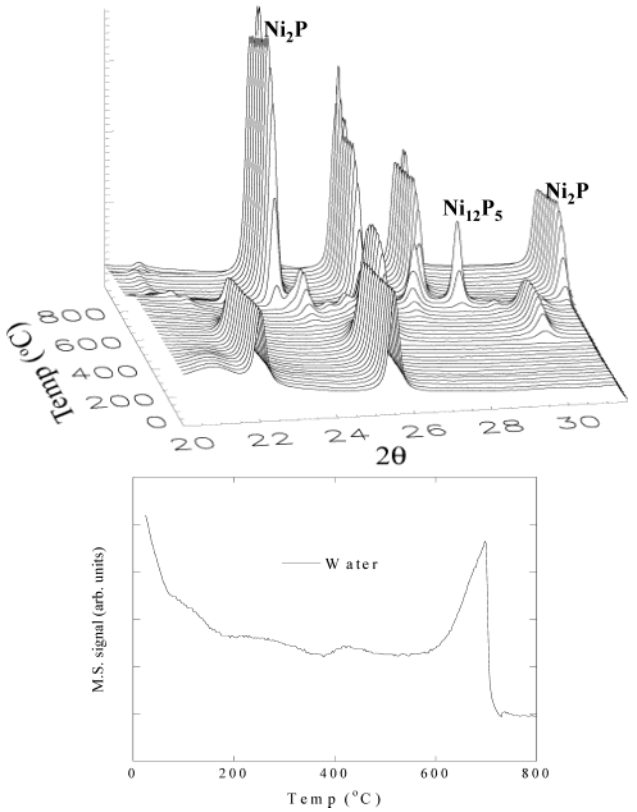

Figure 4. Synthesis of Ni_2P on silica through temperature-programmed reduction. The top panel shows XRD data. The sample was taken from 25 to 800 °C and then cooled back to room temperature. The evolution of water is shown in the bottom panel.

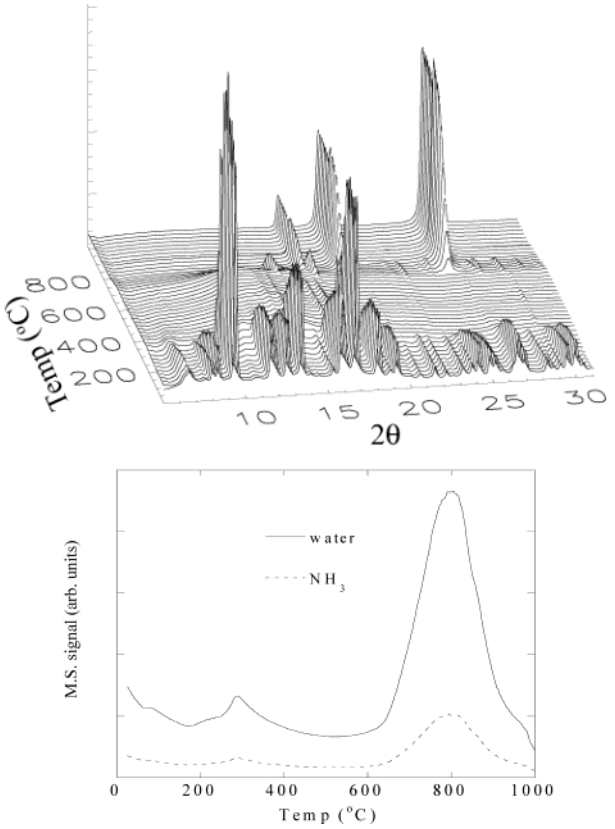

Figure 5. Synthesis of bulk MoP through temperature-programmed reduction. The top panel shows XRD data ($\lambda = 0.9200$ Å). The evolution of water and ammonia is shown in the bottom panel.

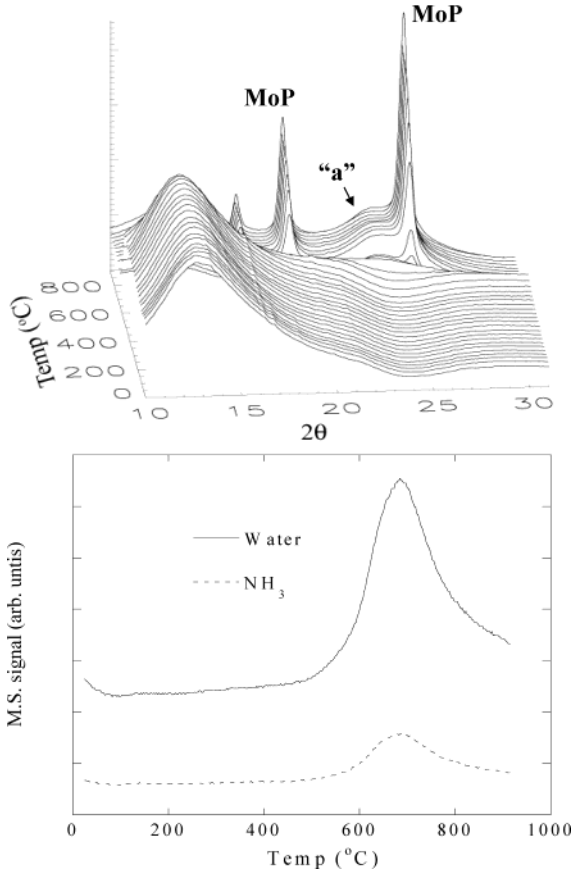

Figure 6. Synthesis of MoP on silica through temperature-programmed reduction. The top panel shows XRD data. The evolution of water and ammonia is shown in the bottom panel.

diffraction peaks for other crystalline compounds were detected and no changes were observed after cooling to room temperature and subsequent heating in flowing He or a 5% H_2/95% He mixture.

The XRD data for the generation of silica-supported molybdenum phosphide (40 wt % MoP) are shown in Figure 6. In this case, the oxidic precursor did not exhibit a well-defined diffraction pattern and only broad features associated with the amorphous silica support were detected. However, upon heating in 5% H_2/95% He, evolution of water and ammonia began near 500 °C and diffraction lines for crystalline MoP appeared. These diffraction lines were not as sharp as in bulk MoP, indicating a limited size (12−14 nm [45]) for the particles of the silica-supported MoP. At the end, in addition to MoP, there was a second species on the silica support (perhaps another phosphide[9]) that produced broad and ill-defined features in the diffraction pattern (labeled "a").

III.3. Synthesis of MoNiP and MoNiP/SiO_2 Catalysts: Conventional and Time-Resolved XRD Studies. For unsupported MoNiP, an oxidic precursor was subjected to TPR under two sets of conditions. In the first case, the oxidic precursor was reduced in a 300 sccm flow of pure H_2 while heating from room temperature to 650 °C (1 °C/min), and the XRD pattern ($\lambda = 1.5418$ Å) for the resulting product is shown in Figure 7. The XRD pattern is in good agreement with a reference pattern for MoNiP[46] and does not show reflections for impurities reported recently by others.[47] For the time-resolved XRD measurements ($\lambda = 0.9200$ Å), the oxidic precursor was subjected to TPR (25−800 °C, 15 °C/min) in a 20 sccm flow of 5% H_2/95% He (Figure 8). When compared to the precursors for Ni_2P and MoP, the precursor for MoNiP did not contain water (i.e., it was not a hydrate) and its diffraction lines (mainly

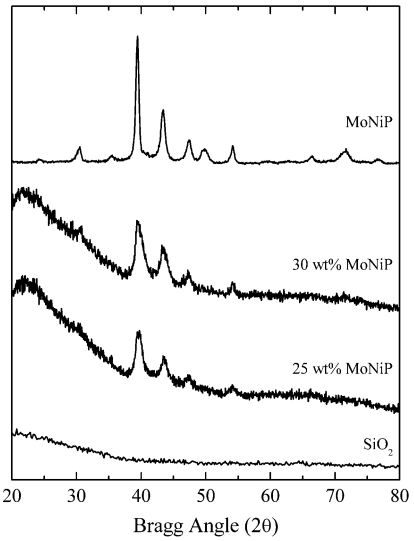

Figure 7. XRD patterns for SiO_2, silica-supported MoNiP catalysts, and bulk MoNiP ($\lambda = 1.5418$ Å).

due to MoO_3[43b]) remained strong up to ∼550 °C, when a sequential reduction process took place giving MoO_2, Mo, and finally MoNiP. Once MoNiP was formed, no modifications occurred in the diffraction pattern upon cooling to room temperature and subsequent heating under a 5% H_2/95% He gas mixture.

At room temperature a complex diffraction pattern (top of Figure 9) was obtained for the oxidic precursor of silica-supported MoNiP (30 wt % MoNiP); overlapping with the broad features for silica were diffraction lines for the precursor of bulk

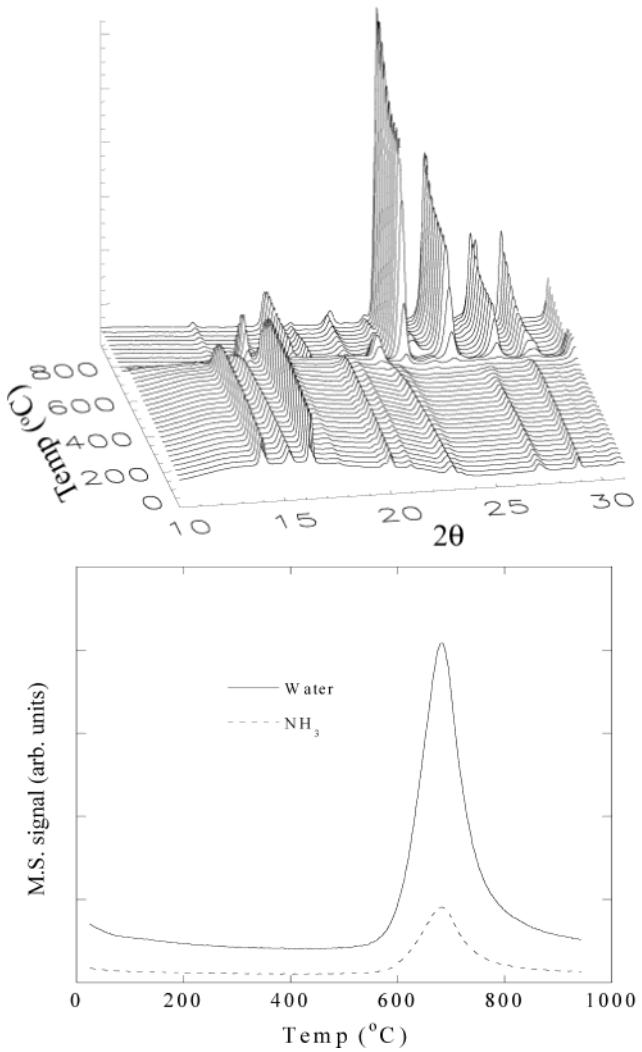

Figure 8. Top: Time-resolved powder diffraction patterns ($\lambda = 0.9200$ Å) for the synthesis of bulk MoNiP through temperature-programmed reduction. The process was performed under a 5% H_2−95% He gas mixture (∼20 cm^3/min flow) with a heating rate of ∼15 °C/min. Bottom: MS signal as a function of temperature for the evolution of water and ammonia.

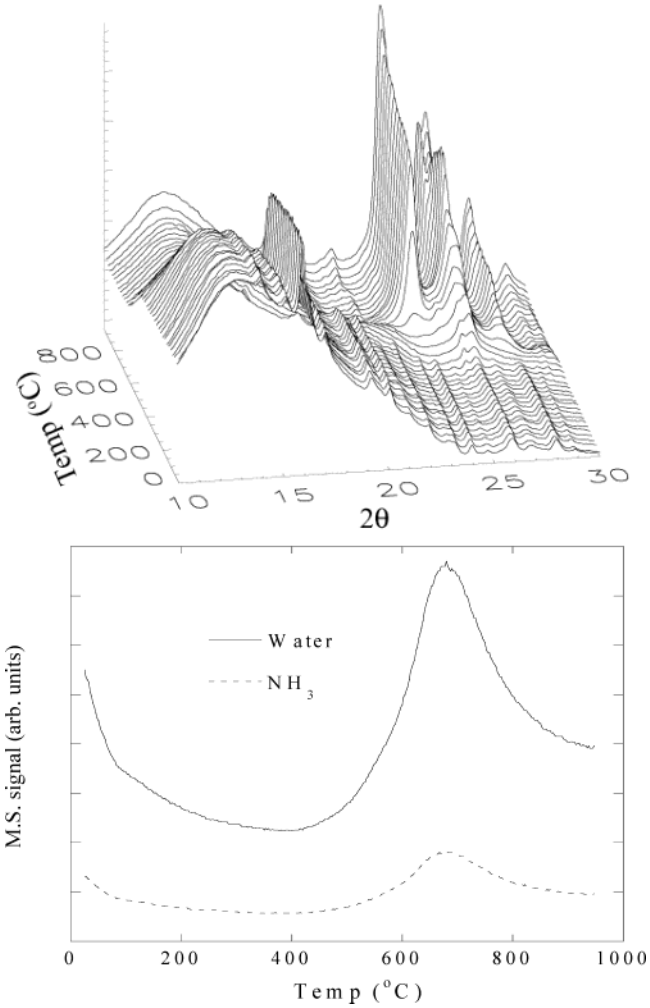

Figure 9. Top: Time-resolved powder diffraction patterns ($\lambda = 0.9200$ Å) for the synthesis of MoNiP on silica through temperature-programmed reduction. The process was performed under a 5% H_2−95% He gas mixture (∼20 cm^3/min flow) with a heating rate of ∼15 °C/min. Bottom: MS signal as a function of temperature for the evolution of water and ammonia.

MoNiP (top of Figure 8), but other crystalline phases as well. Upon reduction in 5% H_2/95% He, this complex system behaved in a way very similar to that seen for the precursor of unsupported MoNiP, and above 600 °C only the broad XRD feature for silica and diffraction lines for MoNiP were detected. The width of these diffraction lines indicated the presence of small (∼8 nm [45]) crystallites of MoNiP on the oxide support.

III.4. Electronic Properties of Ni_2P, MoP, and MoNiP: Density Functional Studies. In previous studies correlations have been found between the electronic properties and HDS activities of metal sulfide catalysts.[48−51] In the current work, density functional calculations were used to investigate the electronic properties of Ni_2P, MoP, and MoNiP. Bulk MoP adopts a crystal structure of the WC type,[52] as shown at the top of Figure 10. The crystal structures of Ni_2P and MoNiP are similar (center and bottom of Figure 10), and both belong to the hexagonal $P\bar{6}2m$ group.[53,54] There are two kinds of nickel atoms in Ni_2P.[53] The Ni atoms near the center of the side faces of the unit cell are replaced with Mo when forming MoNiP.[54]

Table 1 shows experimental and calculated structural parameters for MoP, Ni_2P, and MoNiP. In all cases, the DF calculations predict lattice parameters that agree very well with those determined by X-ray diffraction,[52−54] with errors in the length of the cell axes that are smaller than 2%. The DF calculations indicate that the bonds in the phosphide compounds have a very low degree of ionic character. This can be derived from an analysis of the charge distribution following the Mulliken[37,38] and Hirshfeld[39b] partition schemes. In addition, the valence bands in the phosphides exhibit strong metal (d) and phosphorus (s,p) character. Table 2 lists calculated Mulliken charges. The two types of Ni atoms in Ni_2P have opposite charges, but the charges are quite small in absolute terms. Thus, the Ni−P bonds are best described as covalent. The same is valid for the Mo−P bonds in MoP and MoNiP. When compared to MoS_2, the metal atoms in MoP, Ni_2P, and MoNiP have almost insignificant positive charges. This difference is important[50] and should make the phosphides more reactive toward thiophene than MoS_2.

Figure 11 displays density-of-state (DOS) plots for the occupied bands of Ni_2P and NiMoP. In these isostructural compounds the states near the Fermi level contain metal d and phosphorus p character. From −1 to −4 eV appear the metal d bands, with the phosphorus p (−5 to −9 eV) and s bands (−12 to −15 eV) located deeper in energy. Below the Fermi level, the DOS of metal d states is much larger for Ni_2P than for MoNiP. This can have a direct impact on the chemical reactivity

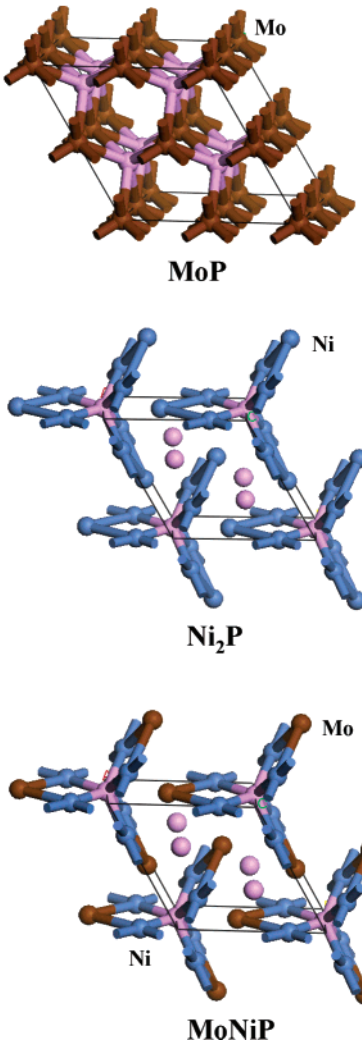

Figure 10. Crystal structures for bulk MoP, Ni_2P, and MoNiP.

TABLE 1: Phosphide Structural Parameters: DF−GGA and XRD Results

axis	MoP	Ni_2P	MoNiP
a (Å)	3.286 (3.223)[a]	5.855 (5.866)	5.832 (5.861)
c (Å)	3.146 (3.191)	3.339 (3.389)	3.729 (3.704)
c/*a*	0.954 (0.990)	0.570 (0.578)	0.639 (0.632)

[a] Values in parentheses come from XRD studies for MoP,[48] Ni_2P,[49] and MoNiP.[50]

TABLE 2: Phosphides and Sulfides: Calculated Charges

	charge (*e*)	
compound	metal[a]	phosphorus
MoP	0.09	−0.09
Ni_2P	−0.08 0.06	0.02[b]
MoNiP	−0.07 (Ni) 0.03 (Mo)	0.04[b]
MoS_2	0.38	

[a] Corresponds to Mo or Ni. [b] Average value.

of the phosphides,[55] especially when dealing with the adsorption of molecules like thiophene where interactions with the LUMO of the adsorbate determine dissociation.[49,50]

III.5. Thiophene HDS Activity. The thiophene HDS activities of silica-supported Ni_2P, MoP, and MoNiP over a 110 h period are shown in Figure 12. For comparison purposes, the HDS activities of sulfided Mo/SiO_2 and $Ni-Mo/SiO_2$ (Ni/Mo = 0.5) catalysts are also shown in the figure; the Mo loading of these catalysts (30.4 wt % MoO_3) is similar to that of the MoP/SiO_2 catalyst. The HDS activities of the catalysts after 100 h on stream are listed in Table 3. The phosphide catalysts were pretreated only by degassing at room temperature for 30 min in flowing He and then heating to the reaction temperature of 370 °C in continued He flow as reported elsewhere.[9,10] The Ni_2P/SiO_2 and MoP/SiO_2 catalysts are significantly more active than the sulfided Mo/SiO_2 and $Ni-Mo/SiO_2$ (Ni/Mo = 0.5) catalysts. Surprisingly, however, the $MoNiP/SiO_2$ catalyst is much less active than the monometallic phosphide catalysts and has an HDS activity between that of the sulfided Mo/SiO_2 and $Ni-Mo/SiO_2$ catalysts. The low HDS activity of the $MoNiP/SiO_2$ catalyst cannot be traced to its dispersion as it has a higher O_2 chemisorption capacity than either the Ni_2P/SiO_2 or the MoP/SiO_2 catalyst. To our knowledge, there have been no other

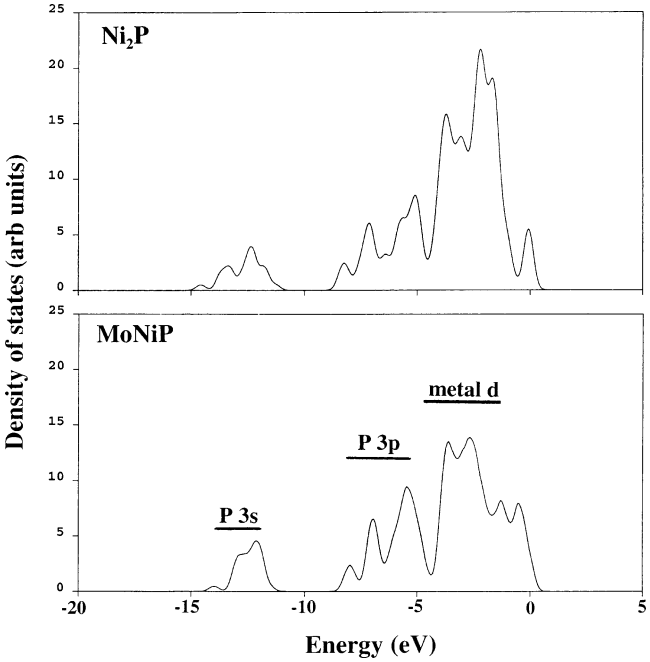

Figure 11. Calculated density of states (DOS) for the occupied valence bands of Ni_2P and MoNiP. The zero of energy is the Fermi level of the system.

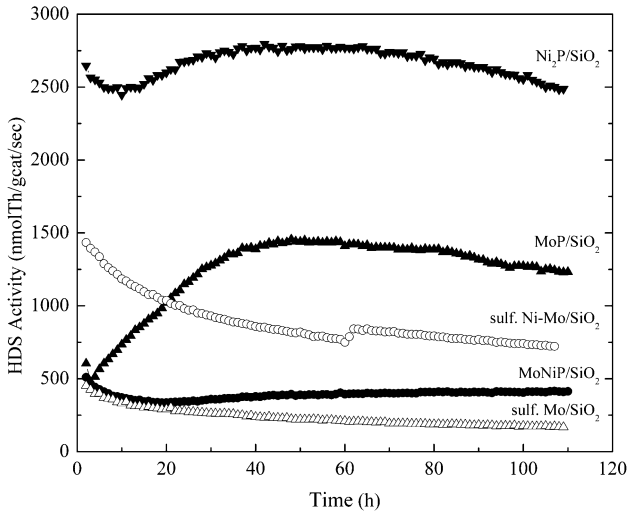

Figure 12. Comparison of the thiophene HDS activities for 30 wt % Ni_2P/SiO_2, 25 wt % MoP/SiO_2, 30 wt % $MoNiP/SiO_2$, sulfided Mo/SiO_2 (30.4 wt % MoO_3), and sulfided $Ni-Mo/SiO_2$ (7.9 wt % NiO, 30.4 wt % MoO_3, Ni/Mo = 0.5) catalysts.

TABLE 3: Data for Phosphide and Sulfide Catalysts

catalyst	BET surf. area (m^2/g)	chemisorption capacity (μmol of O_2/g)	HDS activity (nmol of Th/(g of cat.·s))
30 wt % Ni_2P/SiO_2	66.1	166.1	2562
25 wt % MoP/SiO_2	64.7	119.6	1274
30 wt % $NiMoP/SiO_2$	99.1	184.6	405
sulfided Mo/SiO_2[a]	91.5	18.1	173
sulfided $Ni-Mo/SiO_2$[b]	96.4	22.8	742

[a] The loading of the oxidic precursor was 30.4 wt % MoO_3. [b] The loading of the oxidic precursor was 7.9 wt % NiO, 30.4 wt % MoO_3 (Ni/Mo = 0.5).

reports in the literature of HDS activities of bulk or supported MoNiP catalysts. Stinner et al.[17] measured the *o*-propylaniline hydrodenitrogenation (HDN) activity of unsupported MoNiP and observed it to be less active than either unsupported Ni_2P or MoP.

IV. Discussion

IV.1. Synthesis of Bulk and Silica-Supported Ni_2P, MoP, and MoNiP. As indicated by the time-resolved XRD data in Figures 1, 3−6, 8, and 9, the formation of the metal phosphides occurs at temperatures between 600 an 800 °C. This is independent of the type of oxidic precursor used or the presence of silica as a support. Since the common species in all the cases are phosphate-type groups (PO_x), it seems that their reduction by hydrogen is the final and determining step in the formation of Ni_2P, MoP, and MoNiP. This is clearly seen in Figure 4 for the synthesis of silica-supported Ni_2P. The reduction of the supported NiO produces Ni near 400 °C, but the formation of $Ni_{12}P_5$ and finally Ni_2P does not occur until 550 °C after phosphorus becomes available via the reduction of PO_x groups. The temperature range for the evolution of water in Figure 4 (400−700 °C) matches well with that found in previous studies for the synthesis of silica-supported Ni_2P.[8a] In fact, during the synthesis of other supported phosphides (MoP, Fe_2P, CoP) via the H_2 reduction of oxidic precursors, water evolves into the gas phase at temperatures similar (400−750 °C)[7d,8a] to those observed in the current work.

The time-resolved XRD data in Figure 3 indicate that α-$Ni_2P_2O_7$ can be used as an oxidic precursor for the synthesis of Ni_2P via reduction with hydrogen. In previous studies, $NH_4NiPO_4 \cdot nH_2O$[8a,10] and $Ni_3(PO_4)_2$[56] have been used as precursors in the preparation of Ni_2P. All these systems have in common the need for a large reduction in the oxidation state of phosphorus, and simultaneously there must be a decrease in the P/Ni atomic ratio. These requirements are probably satisfied by a reduction of PO_x groups in hydrogen at high temperature[8a,56] together with a loss of phosphorus as PH_3 and/or P_2O_5.[8a]

For the hydrate and hydroxo precursors used in the synthesis of Ni_2P (Figure 1, $NH_4NiPO_4 \cdot nH_2O$) and MoP (Figure 4, $Mo(OH)_3PO_4$), respectively, the evolution of water and the collapse of the crystal structure occur at temperatures (200−400 °C) similar to those observed for the dehydration of molybdate precursors ($CoMoO_4 \cdot nH_2O$, $NiMoO_4 \cdot nH_2O$) used for the synthesis of molybdenum sulfide catalysts via reduction in H_2/H_2S mixtures.[19,57] In the preparation of the sulfide catalysts, the slow step is the reduction of the oxide precursor,[57] which occurs at lower temperatures (<700 °C)[13,27,57] than those found here for the reduction of phosphate groups.

An important issue in the preparation of supported metal phosphides is the type of phosphide phase formed as a function of temperature and how this is affected by the oxide support. In principle, phosphide↔oxide interactions can enhance the stability of phosphide phases which are metastable or unimportant for the unsupported material. Evidence for the occurrence of such a phenomenon is found in the XRD data of Figure 4 for the synthesis of silica-supported Ni_2P. Before the appearance of Ni_2P, strong diffraction lines are observed for $Ni_{12}P_5$. These lines have a negligible intensity during the synthesis of bulk Ni_2P (Figure 1). In the case of the synthesis of silica-supported MoP (Figure 6), broad diffraction features (labeled "a") are seen at the end, which do not belong to bulk MoP (Figure 5). The existence of silica-stabilized phosphide phases can have an effect on the catalytic properties of these materials. For example, Ni_2P/SiO_2 catalysts containing a $Ni_{12}P_5$ impurity have been observed to have significantly lower HDN[8d] and HDS[10] activities than phase pure, silica-supported Ni_2P.

IV.2. HDS Activity and Electronic Properties of the Phosphides. Silica-supported Ni_2P and MoP exhibit higher HDS activities than MoS_2-based catalysts.[7d,8a,c,9,10] Thus, Ni_2P/SiO_2 and MoP/SiO_2 catalysts have been recently reported to have thiophene HDS activities 15 and 4 times higher, respectively, than sulfided Mo/SiO_2 catalysts when activities are normalized on the basis of catalyst mass.[9,10] In principle, geometric and electronic factors could be responsible for these variations in activity. The trend in catalytic activity can be understood if one takes into consideration the different electronic properties shown in Table 2 and Figure 11 for the metal cations of Ni_2P, MoP, and MoS_2. In previous studies correlations have been found between the electronic properties and HDS activities of metal sulfide catalysts.[48−51] The LUMO of thiophene is C−S antibonding.[50,58] Surfaces that are able to transfer electron density into this orbital facilitate the dissociation of the thiophene molecule.[49,50,58−60] Thus, C_4H_4S readily decomposes on many transition-metal surfaces.[6,61−63] C−S bond scission occurs below −70 °C on Ni(111)[63] and Mo(110).[62] In fact, the bonding interactions between these metals and thiophene or its decomposition products are so strong that the pure metals are useless as HDS catalysts.[3−6,61] In the other extreme are the weak interactions between oxides (Al_2O_3,[64] ZnO,[59] TiO_2[60]) and thiophene. The high ionicity typical of oxides leads to metal centers with a high positive charge and a low density of states near the Fermi level. This produces poor bonding interactions with the LUMO of thiophene,[59,60] and the molecule usually desorbs intact from oxide surfaces at temperatures below 25 °C.[59,60,64] Phosphides and sulfides are an intermediate case between metals and oxides. In Table 2, the charges on the metal cations in bulk Ni_2P and MoP are much smaller than in bulk MoS_2. An identical trend is found in semiempirical quantum-chemical (INDO[50]) calculations for $Ni_{30}P_{15}$, $Mo_{30}P_{30}$, and $Mo_{30}S_{60}$ nanoclusters.[65] Therefore, the metal cations of Ni_2P and MoP probably interact better with the LUMO of thiophene than do those of MoS_2. Furthermore, since Ni_2P has a larger density of metal d states near the Fermi level than MoP, the nickel phosphide should be more reactive.[55] From these differences in the electronic properties the following order of HDS activities can be expected: $MoS_2 < MoP < Ni_2P$, which agrees well with the experimental observations shown in Figure 12.

The crystal structure of MoNiP is obtained after replacing half the nickel atoms in Ni_2P with molybdenum atoms (Figure 10).[54] This exchange leads to a reduction in the density of metal d states near the Fermi level (Figure 11), which is expected to make MoNiP less chemically active than Ni_2P. Indeed, this is what is observed in the HDS data plotted in Figure 12. However, it is not clear why MoNiP is less active than MoP catalysts. For sulfide catalysts, the addition of Ni to Mo-based catalysts

results in a substantial increase in the HDS and HDN activities of the catalysts.[3] The surprising result that silica-supported MoNiP has a lower HDS activity than Ni_2P and MoP on the same support is consistent with HDN studies on the unsupported materials.[17] In our study, the low activity of MoNiP cannot be traced to the relative dispersion or surface area of the catalysts (Table 3). Instead, we may be dealing with a change in the phosphide chemical properties as a result of interactions with the silica support. A Scherrer analysis of the XRD data[45] indicates that the mean crystallite size for the supported phosphides varies from ~28 nm in Ni_2P to ~13 nm in MoP and to ~8 nm in MoNiP. The relatively small particle size in $MoNiP/SiO_2$ may make this system very sensitive to interactions with the oxide support. In previous work, it has been found that the HDS activity of small metal carbide particles can be significantly decreased as a consequence of interactions with an oxide support.[66,67] Clearly, a more comprehensive study of supported MoNiP catalysts will be necessary to fully understand its hydrodesulfurization properties.

V. Conclusions

Synchrotron-based time-resolved X-ray diffraction was used to study in situ the crystalline phases present during the preparation of bulk and silica-supported MoP, Ni_2P, and MoNiP from oxidic precursors. Independent of the type of oxidic precursor used or the presence of silica as a support, the formation of the metal phosphides occurs at temperatures between 600 and 800 °C. Since the common species in all the cases are phosphate-type groups (PO_x), it seems that their reduction by hydrogen is the final and determining step in the formation of MoP, Ni_2P, and MoNiP.

Silica-stabilized phosphide phases were detected during the synthesis of Ni_2P/SiO_2 and MoP/SiO_2 catalysts. In the case of Ni_2P/SiO_2, before the appearance of the final phosphide, strong diffraction lines were observed for $Ni_{12}P_5$. The time-resolved XRD data indicate that α-$Ni_2P_2O_7$ can be used as an oxidic precursor for the synthesis of bulk Ni_2P via reduction with hydrogen.

First-principles density functional calculations for bulk Ni_2P, MoP, and MoNiP indicate that the Ni−P and Mo−P bonds in these compounds have a small degree of ionic character. For Ni_2P, MoP, and MoS_2, a correlation is found between the electronic properties of the metal cations and their HDS activities as silica-supported catalysts. Surprisingly, a $MoNiP/SiO_2$ catalyst is much less active than either MoP/SiO_2 or Ni_2P/SiO_2 catalysts. This could be a consequence of strong interactions with the silica support due to the small size (~8 nm) of the supported MoNiP particles relative to the supported Ni_2P and MoP catalysts.

Acknowledgment. This research was supported by the Division of Chemical Sciences, Office of Basic Energy Sciences, of the US Department of Energy (DOE) and by the National Science Foundation (NSF). The work at BNL was performed under Contract No. DE-AC02-98CH10886. The NSLS is supported by the Divisions of Materials and Chemical Sciences of DOE. The work at WWU was supported by the NSF under Grant CHE-0101690.

References and Notes

(1) Speight, J. G. *The Chemistry and Technology of Petroleum*, 2nd ed.; Dekker: New York, 1991.

(2) Stern, A. C.; Boubel, R. W.; Turner, D. B.; Fox, D. L. *Fundamentals of Air Pollution*, 2nd ed.; Academic Press: Orlando, FL, 1984.

(3) Topsøe, H.; Clausen, B. S.; Massoth, F. E. *Hydrotreating Catalysis*; Springer-Verlag: New York, 1996.

(4) Thomas, J. M.; Thomas, W. J. *Principles and Practice of Heterogeneous Catalysis*; VCH: New York, 1997.

(5) (a) Chianelli, R. R.; Lyons, J. E.; Mills, G. A. *Catal. Today* **1994**, *22*, 361. (b) Chianelli, R. R.; Berhault, G. *Catal. Today* **1999**, *53*, 357.

(6) Rodriguez, J. A.; Hrbek, J. *Acc. Chem. Res.* **1999**, *32*, 719.

(7) (a) Li, W.; Dhandapani, B.; Oyama, S. T. *Chem. Lett.* **1998**, 207. (b) Oyama, S. T.; Clark, P.; Teixiera da Silva, V. L. S.; Lede, E. J.; Requejo, F. G. *J. Phys. Chem. B* **2001**, *105*, 4961. (c) Clark, P.; Li, W.; Oyama, S. T. *J. Catal.* **2001**, *200*, 140. (d) Clark, P.; Wang, X.; Oyama, S. T. *J. Catal.* **2002**, *207*, 256.

(8) (a) Wang, X.; Clark, P.; Oyama, S. T. *J. Catal.* **2002**, *208*, 321. (b) Oyama, S. T.; Clark, P.; Wang, X.; Shido, T.; Iwasawa, Y.; Hayashi, S.; Ramallo-Lopez, J. M.; Requejo, F. G. *J. Phys. Chem. B* **2002**, *106*, 1913. (c) Oyama, S. T.; Wang, X.; Requejo, F. G.; Sato, T.; Yoshimura, Y. *J. Catal.* **2002**, *209*, 1. (d) Oyama, S. T.; Wang, X.; Lee, Y. K.; Bando, K.; Requejo, F. G. *J. Catal.* **2002**, *210*, 207.

(9) Phillips, D. C.; Sawhill, S. J.; Self, R.; Bussell, M. E. *J. Catal.* **2002**, *207*, 266.

(10) Sawhill, S. J.; Phillips, D. C.; Bussell, M. E. *J. Catal.* **2003**, in press.

(11) Norby, P.; Hanson, J. C. *Catal. Today* **1998**, *39*, 301, and references therein.

(12) Rodriguez, J. A.; Hanson, J. C.; Frenkel, A. I.; Kim, J. Y.; Pérez, M. *J. Am. Chem. Soc.* **2002**, *124*, 346.

(13) Rodriguez, J. A.; Kim, J.-Y.; Hanson, J. C.; Brito, J. L. *Catal. Lett.* **2002**, *82*, 103.

(14) Rodriguez, J. A.; Hanson, J. C.; Kim, J.-Y.; Liu, G.; Iglesias-Juez, A.; Fernández-García, M. *J. Phys. Chem. B* **2003**, *107*, 3535.

(15) Rodriguez, J. A.; Kim, J.-Y.; Hanson, J. C.; Pérez, M.; Frenkel, A. I. *Catal. Lett.* **2003**, *85*, 247.

(16) Gopalakrishnan, J.; Pandey, S.; Rangan, K. K. *Chem. Mater.* **1997**, *9*, 2113.

(17) Stinner, C.; Prins, R.; Weber, T. *J. Catal.* **2001**, *202*, 187.

(18) Aegerter, P. A.; Quigley, W. W. C.; Simpson, G. J.; Ziegler, D. D.; Logan, J. W.; McCrea, K. R.; Glazier, S.; Bussell, M. E. *J. Catal.* **1996**, *164*, 109.

(19) Rodriguez, J. A.; Chaturvedi, S.; Hanson, J. C.; Albornoz, A.; Brito, J. L. *J. Phys. Chem. B* **1998**, *102*, 1347.

(20) Rodriguez, J. A.; Hanson, J. C.; Chaturvedi, S.; Maiti, A.; Brito, J. L. *J. Chem. Phys.* **2000**, *112*, 935.

(21) Hastings, J. B.; Suortii, P.; Thomsolin, P.; Kvick, A.; Koetzle, T. *Nucl. Instrum. Methods* **1983**, *208*, 55.

(22) Chupas, P. J.; Ciraolo, M. F.; Hanson, J. C.; Grey, C. P. *J. Am. Chem. Soc.* **2001**, *123*, 1694.

(23) Clausen, B. S.; Steffensen, G.; Fabius, B.; Villadsen, J.; Freidenhans, R.; Topsre, H. *J. Catal.* **1991**, *132*, 524.

(24) Hammersely, A. P.; Svensson, S. O.; Thompson, A. *Nucl. Instrum. Methods Phys. Res.* **1994**, *346*, 321.

(25) Larson, A. C.; von Dreele, R. B. *GSAS General Structure Analysis System*, Report LAUR 86-748; Los Alamos National Laboratory: Los Alamos, NM, 1995.

(26) Norby, P.; Pashni, F. I.; Gualtieri, A. F.; Hanson, J. C.; Grey, C. P. *J. Phys. Chem. B* **1998**, *102*, 839.

(27) Rodriguez, J. A.; Hanson, J. C.; Chaturvedi, S.; Maiti, A.; Brito, J. L. *J. Phys. Chem. B* **2000**, *104*, 8145.

(28) (a) Payne, M. C.; Allan, D. C.; Arias, T. A.; Johannopoulus, J. D. *Rev. Mod. Phys.* **1992**, *64*, 1045. (b) Milman, V.; Winkler, B.; White, J. A.; Pickard, C. J.; Payne, M. C.; Akhmatskaya, E. V.; Nobes, R. H. *Int. J. Quantum Chem.* **2000**, *77*, 895.

(29) (a) Rodriguez, J. A.; Etxeberria, A.; González, L.; Maiti, A *J. Chem. Phys.* **2002**, *117*, 2699. (b) Rodriguez, J. A.; García, J.; González, L. *Chem. Phys. Lett.* **2002**, *365*, 380.

(30) Sorescu, D. C.; Yates, J. T. *J. Phys. Chem. B* **1998**, *102*, 4556.

(31) Rodriguez, J. A.; Maiti, A. *J. Phys. Chem. B* **2000**, *104*, 3630.

(32) Refson, K.; Wogelius, R. A.; Fraser, D. G.; Payne, M. C.; Lee, M. H.; Milman, V. *Phys. Rev. B* **1995**, *52*, 10823.

(33) Rodriguez, J. A.; Jirsak, T.; Pérez, M.; Chaturvedi, S.; Kuhn, M.; González, L; Maiti, A. *Am. Chem. Soc.* **2000**, *122*, 12362.

(34) Vanderbilt, D. *Phys. Rev. B* **1990**, *41*, 7892.

(35) Monkhorst, H. J.; Pack, J. D. *Phys. Rev. B* **1976**, *13*, 5188.

(36) Perdew, J. P.; Burke, K.; Ernzerhof, M. *Phys. Rev. Lett.* **1996**, *77*, 3865.

(37) Segall, M. D.; Pickard, C. J.; Shah, R.; Payne, M. C. *Phys. Rev. B* **1996**, *54*, 16317.

(38) Segall, M. D.; Pickard, C. J.; Shah, R.; Payne, M. C. *Mol. Phys.* **1996**, *89*, 571.

(39) (a) Szabo, A.; Ostlund, N. S. *Modern Quantum Chemistry*; McGraw-Hill: New York, 1989. (b) Wiberg, K. B.; Rablen, P. R. *J. Comput. Chem.* **1993**, *14*, 1504.

(40) JCPDS Powder Diffraction File (PDF), International Centre for Diffraction Data, Swarthmore, PA, 2000. Card No. 03-0953.

(41) (a) PDF No. 39-0710. Lukaszewicz, K. *Bull. Acad. Pol. Sci., Ser. Sci. Chim.* **1967**, *15*, 47.

(42) (a) PDF No. 47-1049. (b) PDF No. 04-0850. (c) PDF No. 22-1190.
(43) (a) PDF No. 11-0333. (b) PDF No. 35-0609. (c) PDF No. 32-0671.
(44) PDF No. 24-771.
(45) (a) Scherrer, P. *Gott. Nachr.* **1918**, *2*, 98. (b) Young, R. A. *The Rietveld Method*; IUCr Monographies of Crystallography 5; Oxford University Press: Oxford, 1995.
(46) PDF No. 31-0873.
(47) Stinner, C.; Prins, R.; Weber, T. *J. Catal.* **2001**, *202*, 187.
(48) Harris, S.; Chianelli, R. R. *J. Catal.* **1986**, *98*, 17.
(49) Zonnevylle, M.; Hoffmann, R.; Harris, S. *Surf. Sci.* **1988**, *199*, 320.
(50) Rodriguez, J. A. *J. Phys. Chem. B* **1997**, *101*, 7524.
(51) (a) Aray, Y.; Rodriguez, J.; Vega, D.; Rodriguez-Arias, E. N. *Angew. Chem., Int. Ed.* **2000**, *39*, 3810. (b) Aray, Y.; Rodriguez, J.; Vega, D.; Coll, S.; Rodriguez-Arias, E. N.; Rosillo, F. *J. Phys. Chem. B* **2002**, *106*, 13242.
(52) (a) Schönberg, N. *Acta Chem. Scand.* **1954**, *8*, 226. (b) Rundqvist, S.; Lundström, T. *Acta Chem. Scand.* **1963**, *17*, 37.
(53) Rundqvist, S. *Acta Chem. Scand.* **1962**, *16*, 992.
(54) Guerin, P. R.; Sergent, M. *Acta Crystallogr., Sect. B* **1977**, *33*, 2820.
(55) Hoffmann, R. *Solids and Surfaces: A Chemist's View of Bonding in Extended Structures*; VCH, New York, 1988.
(56) (a) Nozaki, F.; Adachi, R. *J. Catal.* **1975**, *40*, 166. (b) Robinson, W. R. A. M.; van Gestel, J. N. M. *J. Catal.* **1996**, *161*, 539.
(57) Brito, J. L.; Barbosa, A. L. *J. Catal.* **1997**, *171*, 467.
(58) Rodriguez, J. A. *Surf. Sci.* **1992**, *278*, 326.
(59) Jirsak, T.; Dvorak, J.; Rodriguez, J. A. *J. Phys. Chem. B* **1999**, *103*, 5550.
(60) Liu, G.; Rodriguez, J. A.; Hrbek, J.; Long, B. T.; Chen, D. A. *J. Mol. Catal. A.* **2003**, in press.
(61) Friend, C. M.; Chen, D. A. *Polyhedron* **1997**, *16*, 3165.
(62) Rodriguez, J. A.; Dvorak, J.; Jirsak, T. *Surf. Sci.* **2000**, *457*, L413.
(63) Huntley, D. R.; Mullins, D. R.; Wingeier, M. P. *J. Phys. Chem.* **1996**, *100*, 19620.
(64) Quigley, W. W. C.; Yamamoto, H. D.; Aegerter, P. A.; Simpson, G. J.; Bussell, M. E.*Langmuir* **1996**, *12*, 1500.
(65) To be published.
(66) Chen, J. G. Personal communication.
(67) Chen, J. G. *Chem. Rev.* **1996**, *96*, 1477.